Insulin resistance and diabetes caused by genetic or diet-induced KBTBD2 deficiency in mice

Zhao Zhang[a], Emre Turer[a], Xiaohong Li[a], Xiaoming Zhan[a], Mihwa Choi[a], Miao Tang[a], Amanda Press[a], Steven R. Smith[b,c], Adeline Divoux[b,c], Eva Marie Y. Moresco[a], and Bruce Beutler[a,1]

[a]Center for the Genetics of Host Defense, University of Texas Southwestern Medical Center, Dallas, TX 75390; [b]Translational Research institute for Metabolism and Diabetes, Florida Hospital, Sanford Burnham Prebys Medical Discovery Institute, Orlando, FL 32827; and [c]Center for Metabolic Origins of Disease, Sanford Burnham Prebys Medical Discovery Institute, Orlando, FL 32827

Contributed by Bruce Beutler, August 30, 2016 (sent for review August 17, 2016; reviewed by Jean-François Bach and Arthur D. Riggs)

We describe a metabolic disorder characterized by lipodystrophy, hepatic steatosis, insulin resistance, severe diabetes, and growth retardation observed in mice carrying *N*-ethyl-*N*-nitrosourea (ENU)–induced mutations. The disorder was ascribed to a mutation of kelch repeat and BTB (POZ) domain containing 2 (*Kbtbd2*) and was mimicked by a CRISPR/Cas9-targeted null allele of the same gene. *Kbtbd2* encodes a BTB-Kelch family substrate recognition subunit of the Cullin-3–based E3 ubiquitin ligase. KBTBD2 targeted p85α, the regulatory subunit of the phosphoinositol-3-kinase (PI3K) heterodimer, causing p85α ubiquitination and proteasome-mediated degradation. In the absence of KBTBD2, p85α accumulated to 30-fold greater levels than in wild-type adipocytes, and excessive p110-free p85α blocked the binding of p85α-p110 heterodimers to IRS1, interrupting the insulin signal. Both transplantation of wild-type adipose tissue and homozygous germ line inactivation of the p85α-encoding gene *Pik3r1* rescued diabetes and hepatic steatosis phenotypes of *Kbtbd2*$^{-/-}$ mice. *Kbtbd2* was down-regulated in diet-induced obese insulin-resistant mice in a leptin-dependent manner. KBTBD2 is an essential regulator of the insulin-signaling pathway, modulating insulin sensitivity by limiting p85α abundance.

diabetes | insulin resistance | Kbtbd2 | p85α | ubiquitination

The insulin-signaling pathway regulates energy homeostasis by promoting glucose and triglyceride uptake into fat, muscle, and other insulin-sensitive cells, stimulating lipogenesis and inhibiting lipolysis, glycogenolysis, and gluconeogenesis (1, 2). Insulin resistance, present in metabolic disorders including obesity and type 2 diabetes, dysregulates these processes and results in chronic elevation of circulating glucose and lipids. Insulin signaling depends on several downstream pathways, including the phosphoinositol 3-kinase (PI3K) pathway, in which PI3Ks are recruited to the plasma membrane by tyrosine-phosphorylated insulin receptor substrates (IRS1 and 2). PI3Ks catalyze the phosphorylation of phosphoinositide 4,5-bisphosphate (PIP_2) to produce phosphoinositide 3,5-triphosphate (PIP_3). PIP_3 recruits to the cell membrane and activates pleckstrin homology domain-containing proteins, including PDK1 and AKT, ultimately leading to glucose transport, lipid and glycogen synthesis, and regulated gene expression.

Class IA PI3Ks, which mediate signaling from the insulin receptor, are heterodimers of a p85 regulatory subunit and a p110 catalytic subunit (3). Although p85 binds and stabilizes p110, p85 also conformationally inhibits p110 catalytic activity (4–8). On activation by insulin, binding to tyrosine-phosphorylated IRS1 relieves the inhibitory conformation of p85, resulting in activation of p110 catalytic activity (4, 8–10). Previous reports have suggested that when present in the cell in excess of stoichiometric amounts, p110-free p85 can bind to tyrosine-phosphorylated IRS1, sequestering IRS1 from prospective catalytically active p85-p110 heterodimers and thereby inhibiting PI3K (11–13).

Here we report a Cullin-3 (Cul3)-based ubiquitination mechanism that limits p85α protein abundance and is essential for normal insulin signaling.

Results

Diabetes, Lipodystrophy, and Hepatic Steatosis in *teeny* Mice. A phenotype observed among third-generation (G3) C57BL/6J mice homozygous for mutations induced by *N*-ethyl-*N*-nitrosourea (ENU), termed *teeny* (*tny*) (14), was characterized by reduced body size and weight within the first few days and throughout postnatal life (Fig. 1 *A* and *B* and Fig. S1 *A* and *B*). Normal amounts of IGF1 were detected in the serum of homozygous *tny* mice (Fig. S1*C*), which consumed more food and water per gram of body weight and produced more urine than wild-type (WT) mice (Fig. S1 *D*–*F*). Between 4 and 8 wk of age, fasting blood glucose and insulin concentrations increased dramatically in *tny*/*tny* mice compared with WT mice; thereafter, hyperglycemia persisted, whereas insulin levels declined to near those of WT mice (Fig. 1 *C* and *D* and Fig. S1 *G*–*I*). Insulin tolerance testing showed insulin resistance in 8-wk-old *tny*/*tny* mice (Fig. 1*E*). We also found that even at 4 wk of age, liver and inguinal white adipose tissue (iWAT) of *tny*/*tny* mice failed to respond to insulin, as indicated by impaired phosphorylation of AKT Ser473 (Fig. S1*J*). These data demonstrate altered glucose metabolism, characterized by hyperglycemia, hyperinsulinemia, and insulin resistance, in homozygous *tny* mice.

Necropsy revealed that adipose tissue beds of *tny*/*tny* mice were reduced in size relative to those in WT mice, a finding most evident in epididymal white adipose tissue (eWAT) but also apparent in iWAT (Fig. 1 *F* and *G*). Hematoxylin and eosin (H&E) staining revealed irregular and shriveled adipocytes

Significance

We report an essential regulator of insulin sensitivity. Mutations affecting this protein, KBTBD2, cause severe insulin-resistant diabetes, lipodystrophy, hepatic steatosis, and growth retardation. KBTBD2 is the substrate recognition subunit of a ubiquitin ligase, and its essential molecular target is p85α, the regulatory subunit of phosphoinositol-3-kinase. KBTBD2 is highly conserved among vertebrates and expressed in liver, brain, muscle, and adipocytes. In the absence of KBTBD2, p85α levels rise 30-fold in adipocytes, interrupting the insulin signal, which is fully restored by p85α knockout. Transfer of KBTBD2-sufficient adipose tissue to KBTBD2-deficient animals rescues insulin-resistant hyperglycemia. Within adipocytes, KBTBD2 expression is markedly down-regulated in response to a high-fat diet. This appears to be an important cause of the insulin resistance caused by obesity.

Author contributions: Z.Z. and B.B. designed research; Z.Z., E.T., X.L., X.Z., M.C., M.T., A.P., and A.D. performed research; S.R.S. contributed new reagents/analytic tools; Z.Z. and B.B. analyzed data; and Z.Z., E.M.Y.M., and B.B. wrote the paper.

Reviewers: J.-F.B., University Paris Descartes; and A.D.R., Beckman Research Institute of City of Hope.

The authors declare no conflict of interest.

[1]To whom correspondence should be addressed. Email: Bruce.Beutler@UTSouthwestern.edu.

This article contains supporting information online at www.pnas.org/lookup/suppl/doi:10.1073/pnas.1614467113/-/DCSupplemental.

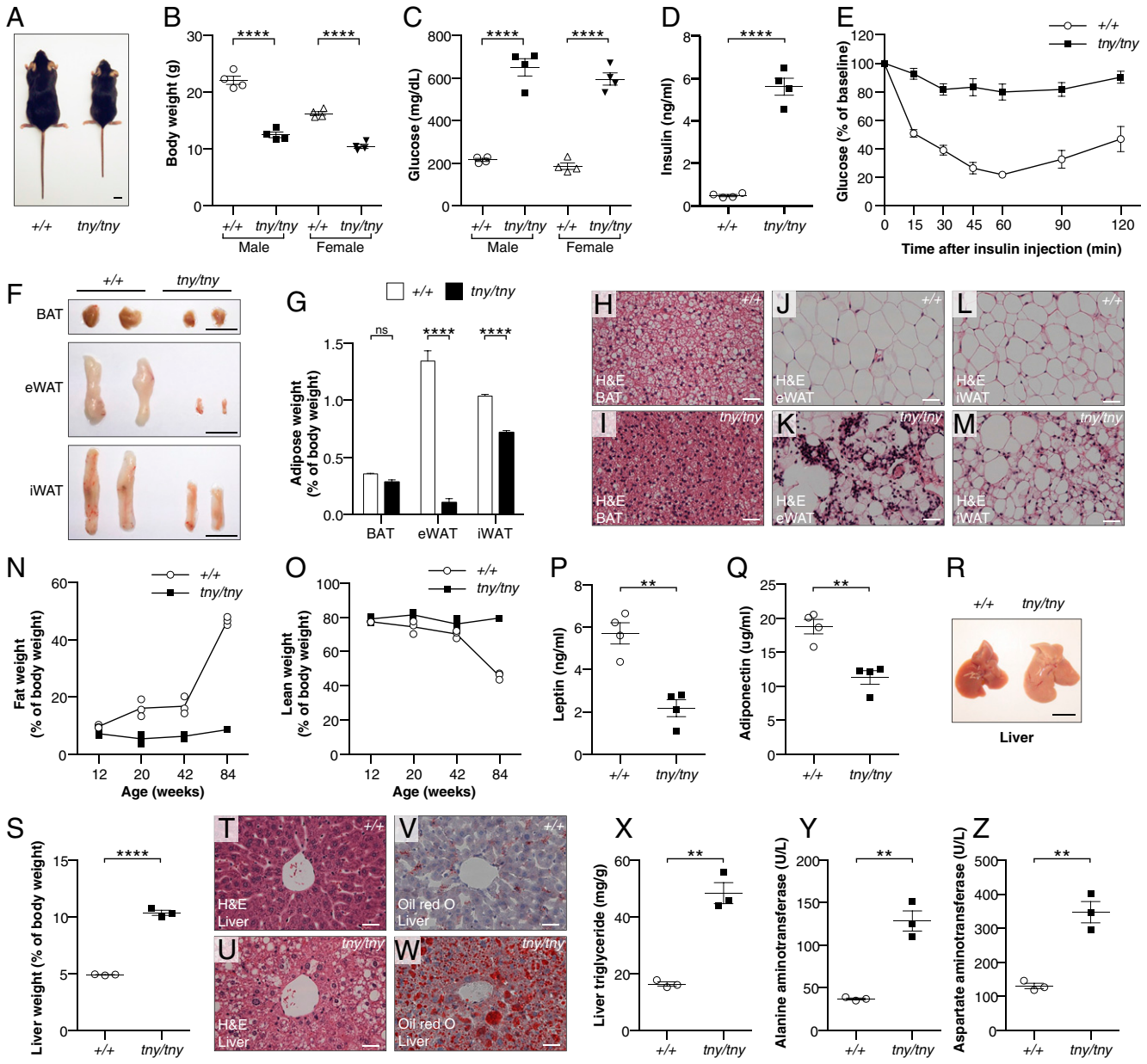

Fig. 1. The *teeny* phenotype. (*A*) Photograph of a male *tny* homozygote (*tny/tny*) and WT (+/+) littermate at 8 wk of age. (Scale bar: 1 cm.) (*B–D*) Body weight (*B*), blood glucose (*C*), and serum insulin (*D*) of 8-wk-old mice. Glucose and insulin were measured after a 6-h fast. (*E*) Insulin tolerance test. Blood glucose was measured at indicated times after i.p. insulin injection in 8-wk-old male mice ($n = 3$). The baseline blood glucose levels (0 min) of *tny/tny* and WT littermates were 626 ± 31 mg/dL and 168 ± 8 mg/dL, respectively. (*F*) Representative photographs of BAT, eWAT, and iWAT from 20-wk-old male mice. (Scale bars: 1 cm.) (*G*) Weights of BAT, eWAT, and iWAT normalized to body weight in 20-wk-old male mice ($n = 3$). (*H–M*) H&E staining of sections from different adipose tissues of 20-wk-old male mice. (Scale bars: 30 μm.) (*N* and *O*) Fat weight (*N*) and lean weight (*O*) normalized to body weight of male mice at indicated ages by MRI ($n = 3$). (*P* and *Q*) Serum leptin (*P*) and adiponectin (*Q*) in 8-wk-old male mice. (*R*) Representative photographs of liver from 8-wk-old male mice. (Scale bar: 1 cm.) (*S*) Liver weight normalized to body weight in 8-wk-old male mice ($n = 3$). (*T–W*) Liver sections of 20-wk-old male mice stained with H&E (*T* and *U*) and Oil red O (*V* and *W*). (Scale bars: 30 μm.) (*X–Z*) Liver triglyceride (*X*), serum ALT (*Y*), and AST (*Z*) in 8-wk-old male mice. In *B–D*, *N–Q*, *S*, and *X–Z*, data points represent individual mice. *P* values were determined by Student's *t* test.

(Fig. 1 *H–M*). Magnetic resonance imaging (MRI) showed that *tny/tny* mice were lean throughout life compared with WT littermates (Fig. 1 *N* and *O*). Presumably as a result of lipodystrophy, *tny/tny* mice had reduced adipokines, such as leptin and adiponectin, in the serum (Fig. 1 *P* and *Q*). In addition, 8-wk-old *tny* mice had large, pallid livers (Fig. 1 *R* and *S*), and Oil Red O (ORO) staining showed an abundance of stored lipid (Fig. 1 *T–W*), possibly a consequence of compromised adipose tissue fat storage caused by impaired insulin signaling (15). Liver extracts of fasting *tny* mice showed increased stored triglyceride compared with WT mice (Fig. 1*X*). Both aspartate aminotransferase (AST) and alanine aminotransferase (ALT) were increased in the serum of *tny* mice, suggesting liver damage caused by lipid accumulation (Fig. 1 *Y* and *Z*).

Both male and female *tny* homozygotes were infertile; females became pregnant but failed to deliver pups. Crosses of heterozygous mice yielded a non-Mendelian birth ratio among offspring (Table S1), suggesting prenatal attrition of homozygotes.

***Tny* Phenotypes Are Caused by a *Kbtbd2* Mutation.** *Tny* was earlier mapped to a premature stop codon in kelch repeat and BTB (POZ) domain containing 2 (*Kbtbd2*) using body weight as a quantitative

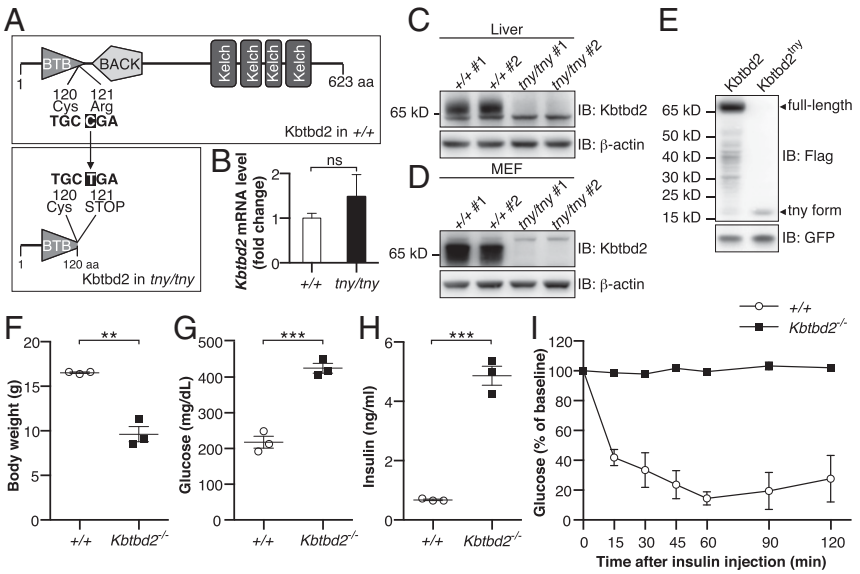

Fig. 2. Mutations of *Kbtbd2* cause the *tny* phenotype. (*A*) Protein domains of WT mouse KBTBD2 (*Upper*) and position of *tny* mutation (*Lower*). The *tny* mutation is an arginine to premature stop codon substitution at position 121 of the protein. (*B*) Relative *Kbtbd2* mRNA level (normalized to *Actb* mRNA) measured by RT-qPCR of mRNA isolated from livers of three male homozygous *tny* mice or WT littermates. (*C* and *D*) Immunoblots of liver (*C*) and MEF (*D*) lysates from two male homozygous *tny* mice and WT littermates. (*E*) Immunoblots of lysates of 293T cells expressing 3×FLAG-tagged full-length WT KBTBD2 or KBTBD2^{tny}. GFP was coexpressed as a loading control. (*F–H*) Body weight (*F*), blood glucose (*G*), and serum insulin (*H*) values in 6-wk-old male homozygous *Kbtbd2* KO (*Kbtbd2*$^{-/-}$) and WT littermates. Glucose and insulin were measured after a 6-h fast. (*I*) Insulin tolerance test. Blood glucose was measured at indicated times after i.p. insulin injection in male *Kbtbd2*$^{-/-}$ mice ($n = 4$) and WT littermates ($n = 3$) at 16 wk of age. The baseline blood glucose levels (0 min) of *Kbtbd2*$^{-/-}$ mice and WT littermates were 728 ± 18 mg/dL and 298 ± 28 mg/dL, respectively. In *F–H*, data points represent individual mice. *P* values were determined by Student's *t* test.

trait under a recessive model of inheritance (Fig. 2*A*) (14). No *tny* phenotypes were observed in heterozygous mice (Fig. S1 *K* and *L*). Although normal levels of *Kbtbd2* mRNA were detected in *Kbtbd2*$^{tny/tny}$ liver (Fig. 2*B*), expression of endogenous KBTBD2 was undetectable by immunoblotting in *Kbtbd2*$^{tny/tny}$ liver or mouse embryonic fibroblast (MEF) lysates (Fig. 2 *C* and *D*), and no full-length protein was detected when a tagged version of KBTBD2^{tny} was overexpressed in 293T cells (Fig. 2*E*). We confirmed that the *tny* phenotype was caused by *Kbtbd2* mutation in mice homozygous for a second null allele of *Kbtbd2*

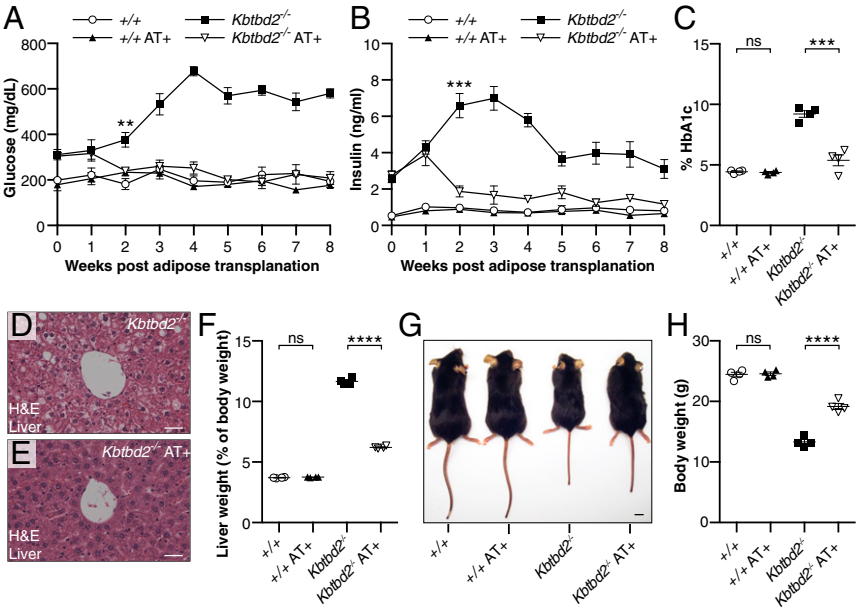

Fig. 3. WT adipose tissue transplantation rescues the *tny* phenotype. Surgery was performed at 4 wk of age, and mice received WT adipose tissue (AT+) or PBS ($n =$ 4 mice of the indicated genotype per condition). (*A* and *B*) Blood glucose (*A*) and serum insulin (*B*) in mice before (0 wk) and at the indicated times after adipose transplantation. (*C*) HbA1c in blood of mice 8 wk after transplantation. (*D* and *E*) H&E staining of sections from liver of *Kbtbd2*$^{-/-}$ or *Kbtbd2*$^{-/-}$ AT+ mice at 12 wk after transplantation. (Scale bars: 30 μm.) (*F–H*) Liver weight normalized to body weight (*F*), representative photograph (*G*), or body weight (*I*) of mice at 12 wk after transplantation. (Scale bar in *G*: 1 cm.) Data points represent individual mice (*C*, *F*, and *H*). *P* values were determined by Student's *t* test.

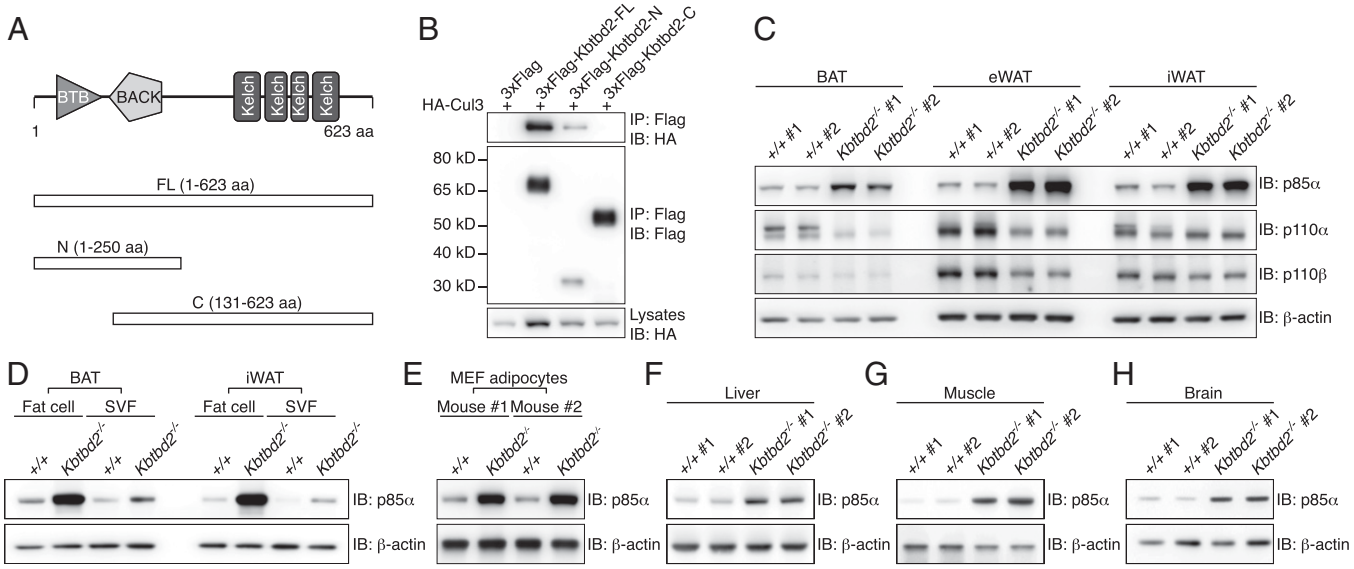

Fig. 4. Elevated p85α Expression in KBTBD2-deficient Mice. (*A*) Protein domains of mouse KBTBD2 and truncated forms for mapping the protein interaction region. (*B*) Immunoblot analysis of immunoprecipitates (*Top* and *Middle*) or lysates (*Bottom*) of 293T cells expressing HA-tagged Cul3 and 3×FLAG-tagged full-length (FL) or truncated KBTBD2. (*C*) Immunoblots of lysates of different adipose tissues from two 8-wk-old male *Kbtbd2*$^{-/-}$ mice or WT littermates. (*D*) Immunoblots of lysates of isolated fat cells or SVF from different adipose tissues of 8-wk-old WT or *Kbtbd2*$^{-/-}$ mice. (*E*) Immunoblots of lysates of 10-d-differentiated MEF-derived adipocytes from two different mice. (*F–H*) Immunoblots of liver (*F*), muscle (*G*), and brain (*H*) lysates from 8-wk-old WT or *Kbtbd2*$^{-/-}$ mice.

generated by CRISPR/Cas9 gene targeting (*Kbtbd2*$^{-/-}$), which fully recapitulated all aspects of the *tny* phenotype (Fig. 2 *F–I*). Taken together, these findings indicate that insulin resistance, diabetes, lipodystrophy, and fatty liver stem from a homozygous null allele of *Kbtbd2* in *tny* mice.

Rescue of the *tny* Phenotype by WT Adipose Tissue. Lipodystrophies are often associated with insulin resistance, diabetes, dyslipidemia, and hepatic steatosis. Thus, we tested whether s.c. implantation of WT adipose tissue into 4-wk-old *Kbtbd2*$^{-/-}$ mice could rescue the hyperglycemia, hyperinsulinemia, and hepatic steatosis observed in these mice. At 12 wk after surgery, transplanted eWAT grafts had a healthy, vascularized appearance, indicating host acceptance of the tissue (Fig. S2). Strikingly, by 2 wk postsurgery, blood glucose and insulin in transplanted *Kbtbd2*$^{-/-}$ mice had decreased to concentrations similar to those in WT mice, and were maintained through 8 wk postsurgery (Fig. 3 *A* and *B*). HbA1c levels were normal in transplanted *Kbtbd2*$^{-/-}$ mice at 8 wk postsurgery (Fig. 3*C*). Moreover, hepatic steatosis in *Kbtbd2*$^{-/-}$ mice was reversed by adipose transplantation (Fig. 3 *D* and *E*); liver weight was similarly restored toward WT levels (Fig. 3*F*). Adipose transplantation also partially rescued the growth retardation of *Kbtbd2*$^{-/-}$ mice (Fig. 3 *G* and *H*). Thus, adipose tissue expressing functional KBTBD2 is by itself sufficient to rescue hyperglycemia, hyperinsulinemia, and hepatic steatosis in *Kbtbd2*$^{-/-}$ mice.

Elevated p85α Expression in KBTBD2-Deficient Mice. The 623-aa KBTBD2 protein, for which no function has been reported previously, contains BTB (Broad-complex, Tramtrack, and Bric à brac) and BACK (BTB and C-terminal Kelch) domains at its N terminus and four tandem Kelch motifs at its C terminus (Fig. 4*A*), similar to other BTB-BACK-Kelch proteins (16). The mouse protein is 98.6% identical to human KBTBD2; highly similar homologs are found in other vertebrates (Table S2), but are not present in invertebrate organisms (17, 18). KBTBD2 was observed both in the nucleus and cytoplasm on overexpression in 293T cells (Fig. S3*A*). *Kbtbd2* mRNA was detected in a variety of mouse tissues, with relatively higher expression in muscle, liver, brain, iBAT, heart, and eWAT (Fig. S3*B*).

Numerous BTB-BACK-Kelch proteins function as substrate recognition components of Cul3-based E3 ubiquitin (Ub) ligase complexes (16, 19). Coimmunoprecipitation (co-IP) experiments showed that full-length KBTBD2 interacted with Cul3 through the KBTBD2 N-terminal BTB domain (Fig. 4 *A* and *B*), suggesting that KBTBD2 might fulfill a similar function. We hypothesized that putative KBTBD2-specified substrates of the Cul3 Ub ligase complex accumulate in *Kbtbd2* mutant mice, and sought to identify these by semiquantitative mass spectrometry analysis of proteins in white adipose tissues of WT or *Kbtbd2*$^{-/-}$ mice. Among the 1,171 proteins identified in all samples (Dataset S1), six proteins were greater than fivefold more abundant in both eWAT and iWAT from *Kbtbd2*$^{-/-}$ mice relative to WT mice (Table S3). p85α, a regulatory subunit of PI3K, was elevated by 40- and 24-fold in *Kbtbd2*$^{-/-}$ eWAT and iWAT, respectively, and we considered it highly relevant to the *tny* phenotype because of its key role in PI3K regulation.

We verified the specific accumulation of p85α in *Kbtbd2*$^{-/-}$ adipose tissues, in which normal to reduced amounts of the PI3K catalytic subunits p110α and p110β were detected (Fig. 4*C*). Within adipose tissues, fat cells accumulated greater amounts of p85α than stromal vascular fraction (SVF) cells (Fig. 4*D*). Similarly, p85α protein accumulated in *Kbtbd2*$^{-/-}$ adipocyte-like cells differentiated from MEFs (MEF-derived adipocytes) (Fig. 4*E*). We observed accumulation of p85α in *Kbtbd2*$^{-/-}$ liver, muscle, and brain (Fig. 4 *F–H*). Knockdown of KBTBD2 in differentiated human adipocytes also increased p85α protein levels (Fig. S4*A*). These data demonstrate that KBTBD2 deficiency results in elevated p85α expression in mouse tissues with high expression levels of *Kbtbd2*, including adipose tissue, liver, muscle, and brain, as well as in human adipocytes.

KBTBD2 Interaction with Cul3 and p85α Results in p85α Ubiquitination. KBTBD2 interacted with p85α when expressed in 293T cells; the p85α inter-SH2 domain (iSH2; Fig. 5 *A* and *B*) and the KBTBD2 C-terminal Kelch domains were required for this interaction (Figs. 4*A* and 5*C*). In vitro GST pull-down experiments supported a direct interaction between KBTBD2 and p85α (Fig. 5*D*). Human KBTBD2 also interacted with human p85α in differentiated adipocytes

(Fig. S4*B*). Moreover, two-step IP demonstrated simultaneous binding of p85α and Cul3 to KBTBD2 to form a three-protein complex (Fig. 5*E*). Coexpression of KBTBD2, p85α, Cul3, and Ub in 293T cells resulted in p85α polyubiquitination, which was reduced in the absence of Cul3 or KBTBD2 (Fig. 5*F*). The BTB domain is critical for the recruitment of Cul3 Ub ligase complexes, because KBTBD2-C failed to mediate p85α ubiquitination (Fig. 5*F*). These polyubiquitin chains were K48-linked (Fig. 5 *F*–*H*), which serves as a degradation signal for the proteasome. These data suggest that KBTBD2 recruits p85α to Cul3 Ub ligase complexes for K48-linked ubiquitination, leading to proteasome-mediated degradation of p85α.

Impaired PI3K Signaling due to Elevated p85α in *Kbtbd2*$^{-/-}$ Mice. Based on its striking rescue of metabolic phenotypes, we focused on adipose tissue to determine the effect of increased p85α expression on insulin signaling. We examined *Kbtbd2*$^{-/-}$ adipose tissue in vivo for the association between PI3K subunits and IRS-1 and AKT S473 phosphorylation before and after i.p. injection of insulin in WT or *Kbtbd2*$^{-/-}$ mice. In WT iWAT, insulin induced tyrosine phosphorylation of IRS-1, and formation of a complex containing IRS-1, p110α, and p85α (Fig. 6*A*). In contrast, IRS-1 was associated with large amounts of p85α in *Kbtbd2*$^{-/-}$ iWAT independent of insulin stimulation, and p110α bound minimally to IRS-1 either before or after insulin stimulation (Fig. 6*A*). Moreover, phosphorylation of AKT S473 increased in WT iWAT after insulin stimulation, but this response was diminished in *Kbtbd2*$^{-/-}$ iWAT (Fig. 6*A*). We also observed increased levels of insulin-independent tyrosine phosphorylation on IRS-1 in *Kbtbd2*$^{-/-}$ iWAT, likely a result of elevated endogenous insulin in the mice (Fig. 6*A*). These data suggest that elevated p85α expression in *Kbtbd2*$^{-/-}$ adipose tissue results in impaired PI3K signaling. These signaling defects are likely adipocyte-intrinsic, given that *Kbtbd2*$^{-/-}$ MEF-derived adipocytes and human adipocytes in which KBTBD2 was knocked down also exhibited impaired AKT S473 phosphorylation in response

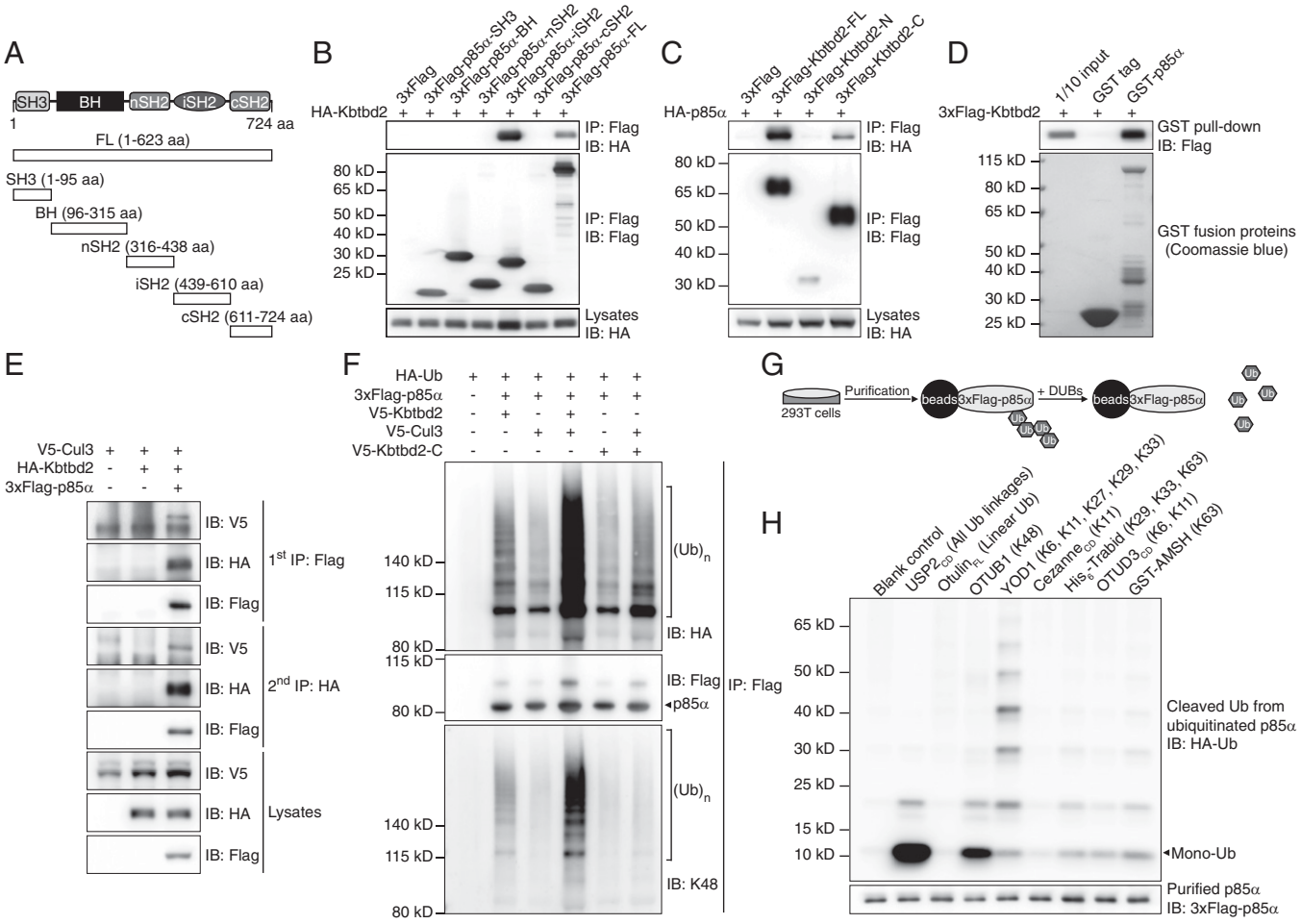

Fig. 5. Interaction of KBTBD2 with Cul3 and p85α results in p85α ubiquitination. (*A*) Protein domains of mouse p85α and truncated forms for mapping the protein interaction region. (*B*) Immunoblot analysis of immunoprecipitates (*Top* and *Middle*) or lysates (*Bottom*) of 293T cells expressing HA-tagged KBTBD2 and 3×FLAG-tagged full-length (FL) or truncated p85α. (*C*) Immunoblot analysis of immunoprecipitates (*Top* and *Middle*) or lysates (*Bottom*) of 293T cells expressing HA-tagged p85α and 3×FLAG-tagged full-length (FL) or truncated KBTBD2. (*D*) Purified 3×FLAG-tagged KBTBD2 was incubated with GST or GST-tagged p85α. After GST pull-down, bound protein was analyzed by FLAG immunoblot (*Top*). The amounts of GST and GST-p85α were visualized by Coomassie blue staining (*Bottom*). (*E*) Immunoblot analysis of lysates of 293T cells expressing the indicated proteins and subjected to two-step IP to detect the three-protein complex. (*F*) IP analysis of lysates of 293T cells expressing HA-tagged Ub and the indicated proteins. (*G*) Flowchart of experimental procedures for data in *H*. HA-tagged Ub and 3×FLAG-tagged p85α were expressed in 293T cells. Immunoprecipitated 3×FLAG-p85α was treated with the indicated deubiquitinating enzymes (DUBs), which specifically cleave particular Ub linkages. The released HA-Ub in the reaction supernatant was immunoblotted with HA antibody. The deubiquitinated 3×FLAG-p85α was immunoblotted with FLAG antibody. (*H*) Immunoblot analysis of HA-tagged Ub (*Top*) released by the indicated DUBs from ubiquitinated 3×FLAG-tagged p85α (*Bottom*). Mono-Ub, monoubiquitin.

to insulin (Fig. 6*B* and Fig. S4*C*). Moreover, the expression of adipocyte differentiation markers PPARγ and C/EBPα was normal in *Kbtbd2*$^{-/-}$ MEF-derived adipocytes and adipose tissues, whereas the expression of fatty acid synthase (FAS) and acetyl-CoA carboxylase (ACC), enzymes involved in fatty acid synthesis, was reduced, suggesting that KBTBD2 deficiency impairs the metabolic function of adipocytes, but not their differentiation (Fig. 6*C* and Fig. S5).

To confirm that elevated p85α was the biological anomaly responsible for the observed PI3K signaling defects and *tny* phenotype, we generated mice deficient in both KBTBD2 and p85α (*Kbtbd2*$^{-/-}$*; Pik3r1*$^{-/-}$). Compared with *Kbtbd2*$^{-/-}$ mice, *Kbtbd2*$^{-/-}$*; Pik3r1*$^{-/-}$ mice had increased body weight, restored fat storage, and decreased blood glucose and insulin (Fig. 6 *D*–*G*). Furthermore, loss of p85α restored insulin sensitivity in the *Kbtbd2*$^{-/-}$ background (Fig. 6*H*). These findings indicate that PI3K signaling in response to insulin is impaired in KBTBD2-deficient mice owing to increased amounts of p85α, and that accumulated p85α causes the *tny* phenotype.

KBTBD2 Suppression Within Adipocytes Occurs in Diet-Induced Obesity. Obesity is strongly associated with insulin resistance (20, 21), and the clear requirement for KBTBD2 in the maintenance of insulin sensitivity prompted us to determine whether KBTBD2 might be modulated by diet-induced obesity. WT C57BL/6J mice maintained on a high-fat diet for 18 wk exhibited higher body weight owing to obesity, increased fasting glucose levels, and insulin resistance (Fig. 7 *A*–*E*). We also observed reduced KBTBD2 mRNA and protein expression and increased p85α protein expression in adipose tissue from these mice (Fig. 7 *F* and *G*). No effect on p85α mRNA was detected (Fig. 7*H*), consistent with posttranslational regulation via the proteasome. These data suggest that KBTBD2 may be modulated by diet-induced obesity.

We also measured KBTBD2 and p85α expression in isolated adipocytes from several genetic mouse models of obesity. Leptin-deficient (Fig. S6 *A*–*E*), leptin receptor-deficient (Fig. S6 *F*–*J*), and melanocortin 4 receptor (Mc4r)-deficient mice (Fig. S6 *K*–*O*) fed a control diet or standard chow were hyperphagic and became obese, hyperglycemic, and insulin-resistant compared with control mice. However, KBTBD2 and p85α mRNA and protein expression levels in the mutants were similar to those in control mice (Fig. 7 *I*–*Q*). To determine whether a high-fat diet could induce suppression of KBTBD2 in the obese mutant mice, *Lep*$^{ob/ob}$ (*ob*/*ob*) mice were fed a high-fat diet for 8 wk, after which the *ob*/*ob* mice were significantly more obese, hyperglycemic, and insulin-resistant than the *ob*/*ob* mice fed the control diet (Fig. S6 *A*–*E*). Nonetheless, KBTBD2 and p85α mRNA and protein levels were similar in the *ob*/*ob* mice fed the control diet and those fed a high-fat diet (Fig. 7 *I*–*K*). These data suggest that leptin receptor signaling is necessary for the regulation of KBTBD2 in diet-induced obesity.

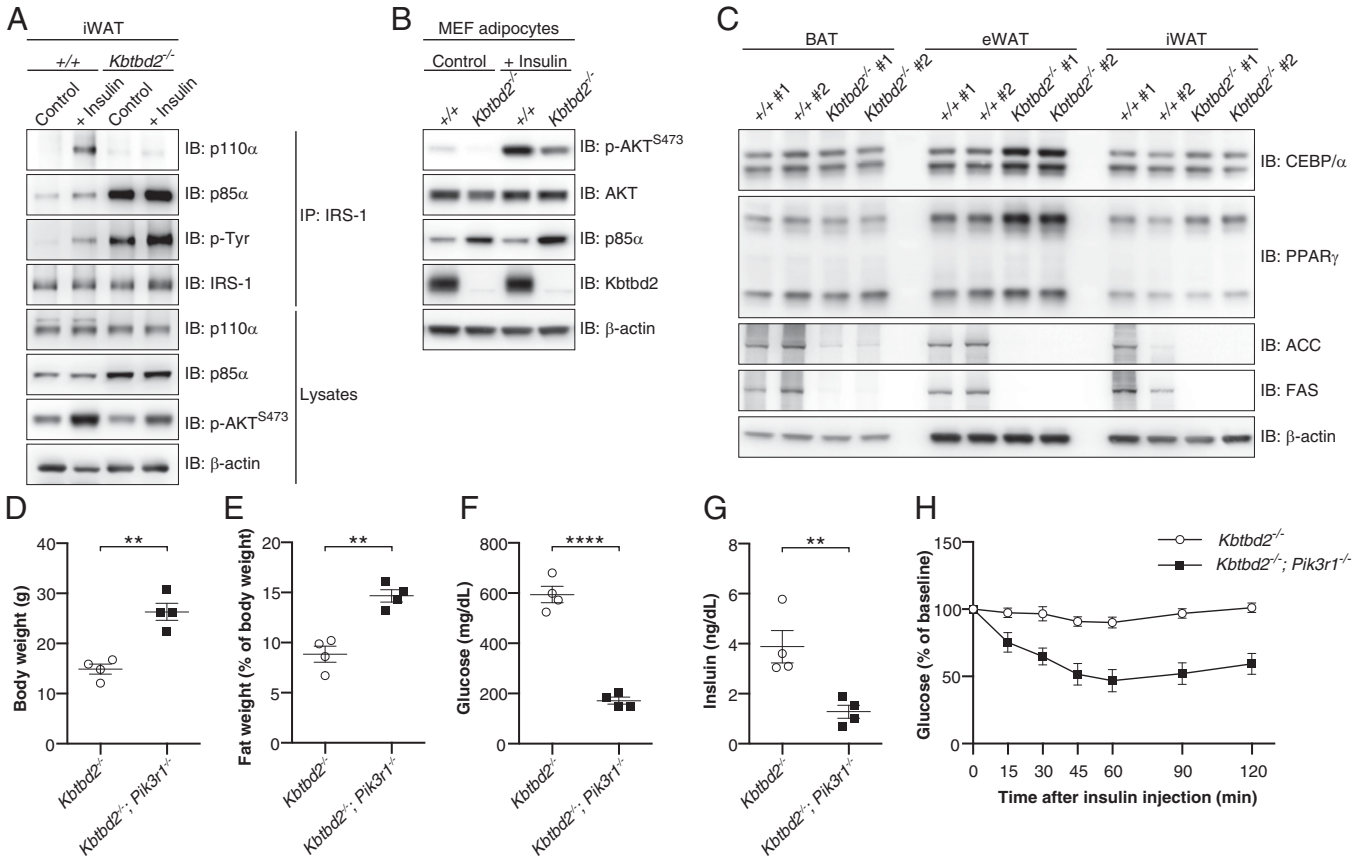

Fig. 6. p85α accumulation impairs PI3K signaling and causes the *tny* phenotype. (*A*) Immunoblot analysis of immunoprecipitates and lysates of iWAT before (Control, anesthesia alone) or 5–6 min after i.v. injection of insulin (+Insulin). (*B*) Immunoblots of lysates of 10-d-differentiated MEF-derived adipocytes. (*C*) Immunoblots of lysates of different adipose tissues from two 8-wk-old male *Kbtbd2*$^{-/-}$ mice or WT littermates. (*D*–*G*) Body weight (*D*), normalized fat weight (*E*), blood glucose levels (*F*), and serum insulin levels (*G*) of 11-wk-old male *Kbtbd2*$^{-/-}$ and *Kbtbd2*$^{-/-}$*; Pik3r1*$^{-/-}$ mice. Glucose and insulin were measured after a 6-h fast. (*H*) Insulin tolerance test. Blood glucose was measured at indicated times after i.p. insulin injection in male *Kbtbd2*$^{-/-}$ mice (n = 4) and *Kbtbd2*$^{-/-}$*; Pik3r1*$^{-/-}$ mice (n = 4) at 11 wk of age. The baseline blood glucose levels (0 min) of *Kbtbd2*$^{-/-}$ mice and *Kbtbd2*$^{-/-}$*; Pik3r1*$^{-/-}$ mice were 594 ± 32 mg/dL and 172 ± 14 mg/dL, respectively. In *D*–*G*, data points represent individual mice. *P* values were determined by Student's *t* test.

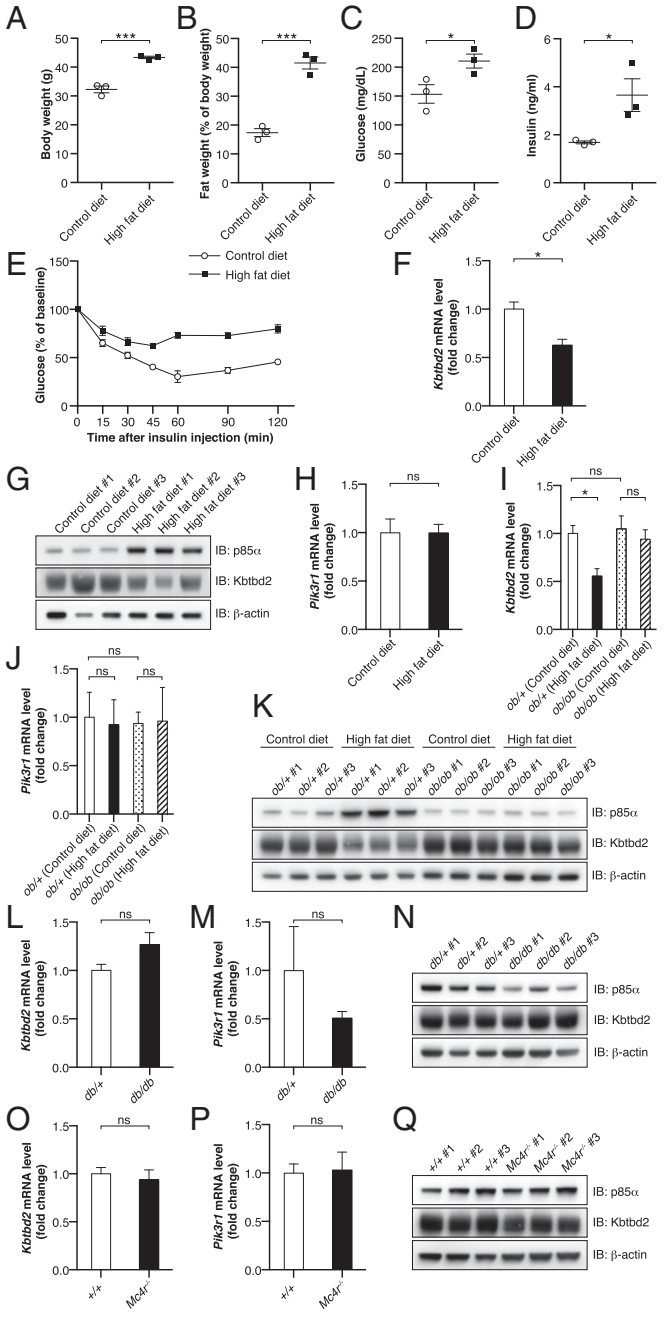

Fig. 7. Down-regulation of KBTBD2 during diet-induced obesity. (*A*–*H*) Male C57BL/6J mice were maintained on a control diet (10 kcal% fat; $n = 3$) or high-fat diet (60 kcal% fat; $n = 3$) for 16 wk, beginning at 6 wk of age. Experiments were conducted at 22 wk of age. (*A*) Body weight. (*B*) Normalized fat weight. (*C*) Blood glucose. (*D*) Serum insulin. Glucose and insulin were measured after a 6-h fast. (*E*) Insulin tolerance test. Blood glucose was measured at indicated times after i.p. insulin injection. The baseline blood glucose levels (0 min) were 154 ± 16 mg/dL in the mice fed the control diet and 211 ± 12 mg/dL in the mice fed the high-fat diet. (*F*) Transcript levels of *Kbtbd2* (normalized to *Actb*) by RT-qPCR of RNA isolated from iWAT. (*G*) Immunoblots of iWAT lysates. (*H*) Transcript levels of *Pik3r1* (normalized to *Actb*) by RT-qPCR of RNA isolated from iWAT. (*I*–*K*) Male $Lep^{ob/+}$ (*ob*/+) or $Lep^{ob/ob}$ (*ob*/*ob*) littermates were maintained on the control diet ($n = 3$) or high-fat diet ($n = 3$) for 8 wk, beginning at 6 wk of age. Experiments were conducted at 14 wk of age. (*I* and *J*) Transcript levels of *Kbtbd2* and *Pik3r1* (normalized to *Actb*) by RT-qPCR of RNA isolated from iWAT. (*K*) Immunoblots of iWAT lysates. (*L*–*N*) Male $Lepr^{db/+}$ (*db*/+; $n = 3$) and $Lepr^{db/db}$ (*db*/*db*; $n = 3$) littermates were maintained on standard chow from birth. Experiments were conducted at 16 wk of age. (*L* and *M*) Transcript levels of *Kbtbd2* and *Pik3r1* (normalized to *Actb*) by RT-qPCR of RNA isolated from iWAT. (*N*) Immunoblots of iWAT lysates. (*O*–*Q*) Male $Mc4r^{-/-}$ mice ($n = 3$) and WT mice (+/+; $n = 3$) were maintained on standard chow from birth. Experiments were conducted at 9 wk of age. (*O* and *P*) Transcript levels of *Kbtbd2* and *Pik3r1* (normalized to *Actb*) by RT-qPCR of RNA isolated from iWAT. (*Q*) Immunoblots of iWAT lysates. In *A*–*D*, data points represent individual mice. *P* values were determined by Student's *t* test.

Discussion

We have shown that KBTBD2 is a p85α-specific recognition subunit for the Cul3-based E3 Ub ligase complex, which regulates p85α protein abundance in vivo (Fig. 8). In particular, KBTBD2 binds exclusively to p110-free p85α, leading to its Ub-mediated degradation. Moreover, in KBTBD2-deficient tissue, excess p85α constitutively precludes the association of p110 with IRS1, resulting in impaired PI3K signaling in response to insulin. Our findings support a model (11–13) in which p110-free p85α competes with the p85α-p110 heterodimer for binding to tyrosine-phosphorylated IRS1 and thereby negatively regulates PI3K signaling. Indeed, a similar mechanism has been reported for the regulation of p85β, which is targeted to SCF Ub ligase complexes by the F-box protein FBXL2 (22). The control of specific p85 isoforms by distinct substrate recognition proteins of Ub ligase complexes suggests a mechanism by which the isoforms may be differentially regulated to carry out nonredundant functions in cells.

It is not excluded that in addition to the insulin receptor, other receptors and pathways linked to activation of the p110 subunit of PI3K are affected by *Kbtbd2* mutations. We note that *tny*/*tny* mice exhibited high levels of serum IGF1, indicative of elevated growth hormone (GH) secretion. IGF1 mediates many of the physiological effects of GH, and also acts as a negative feedback regulator of GH gene expression through the transcription factors POU1F1 and CBP (23–26). These effects occur through signaling primarily via IRS1/IRS2, PI3K, and Akt (26, 27). We hypothesize that IGF1 receptor signaling is also dependent on KBTBD2-induced degradation of p85α, the buildup of which disrupts PI3K signaling and leads to a form of dwarfism and an increase in GH secretion.

In humans, autosomal dominant mutations of *PIK3R1*, encoding p85α and the alternatively spliced isoforms p55α and p50α, cause SHORT syndrome (short stature, hyperextensibility of joints and/or inguinal hernia, ocular depression, Rieger anomaly, and teething delay), a condition also characterized by insulin resistance, lipodystrophy, and impaired PI3K signaling (28–30). The commonality of these latter phenotypes in KBTBD2-deficient mice and SHORT syndrome patients suggests that the human *PIK3R1* mutations exert a dominant negative effect that mimics p85α overexpression. This hypothesis is supported by the autosomal dominant inheritance of reported SHORT syndrome mutations, and also by the observation of insulin hypersensitivity in mice lacking p85α (31–34). In its C-terminal half, p85α contains two SH2 domains separated by a coiled-coil inter-SH2 domain, which together bind p110 or tyrosine-phosphorylated IRS1. The positions of reported SHORT syndrome mutations within p85α SH2 domains or the inter-SH2 domain, but not elsewhere in the protein (28–30), suggest a mechanism in which the mutant p85α proteins may constitutively bind to IRS1, blocking insulin-induced WT p85α-p110 binding. Alternatively, mutant p85α may constitutively bind to p110 in the inhibitory conformation, blocking p110 catalytic activity. Our findings raise the possibility that mutations of KBTBD2 underlie SHORT syndrome in patients without *PIK3R1* mutations.

Among the multiple isoforms of p85, p85α is the predominant isoform in insulin-sensitive tissues (11). p85α-deficient mice exhibit increased insulin signaling, enhanced insulin sensitivity, and hypoglycemia (31–34), whereas p85α overexpression has been reported to reduce PI3K signaling, leading to insulin resistance (35, 36). Consistent with these observations, KBTBD2-deficient

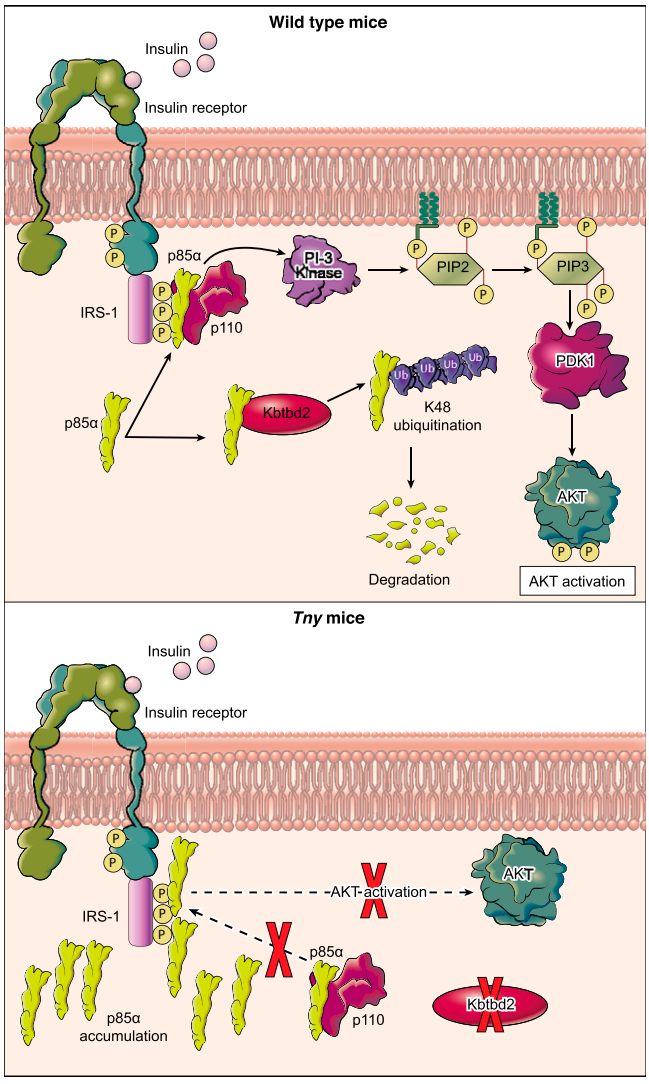

Fig. 8. Regulation of p85α by KBTBD2 in WT and *tny/tny* mice. In WT mice, KBTBD2 regulates p85α protein abundance through degradation mediated by K48 ubiquitination. Insulin induces phosphorylated IRS-1 to recruit p85α-p110 heterodimers, leading to activation of PI3K catalytic activity and downstream signaling. In KBTBD2-deficient *tny/tny* mice, excess p85α constitutively precludes the association of p85-p110 heterodimers with phosphorylated IRS-1, resulting in impaired PI3K signaling in response to insulin.

mice accumulated p85α in adipose, liver, muscle, brain, and possibly other tissues and displayed insulin resistance, diabetes, and liver steatosis. p85α knockout entirely prevented all of these effects of KBTBD2 deficiency. Moreover, transplantation of WT adipose tissue into *Kbtbd2*$^{-/-}$ mice was sufficient to rescue the hyperglycemia and hepatic steatosis phenotypes of these animals, indicating that adipocytes alone are capable of managing the burden of glucose and lipid present in these animals, provided that they have normal insulin sensitivity.

We observed reduced KBTBD2 expression in adipocytes, and consequent elevated adipocyte p85α expression, during high-fat diet-induced obesity associated with insulin resistance and hyperglycemia. These data suggest that diet-induced obesity results in down-regulation of KBTBD2, which may contribute to the development of insulin resistance. Interestingly, no down-regulation of KBTBD2 expression was observed in obese insulin-resistant mice lacking leptin or melanocortin 4 receptor signaling, suggesting that the regulation of KBTBD2 by diet-induced obesity is leptin-dependent. Moreover, a KBTBD2-independent mechanism is apparently responsible for the development of insulin resistance and diabetes in *ob/ob*, *db/db*, and *Mc4r*$^{-/-}$ mice.

The strong evolutionary conservation of KBTBD2 in vertebrates suggests that it may fulfill a similar function in many vertebrate species, in which the need for multiple controls of insulin responsiveness may have developed as organisms increased in complexity from invertebrates. The KBTBD2 protein is 98.6% identical in humans and mice, and we hypothesize that KBTBD2 may regulate systemic insulin sensitivity by controlling the cytoplasmic concentration of p85α in adipose and other tissues in humans as in mice.

Materials and Methods

Mice. C57BL/6J, *Lep*^{ob}, *Lepr*^{db}, and *Mc4r*$^{-/-}$ mice were purchased from The Jackson Laboratory. The *tny* strain (*C57BL/6J-Kbtbd2*^{tny}) was generated by ENU mutagenesis and is described at mutagenetix.utsouthwestern.edu. *Kbtbd2*$^{-/-}$ and *Kbtbd2*$^{-/-}$*; Pik3r1*$^{-/-}$ double-knockout mice were generated in our laboratory using the CRISPR/Cas9 system as described previously (37) with the *Kbtbd2* (5′-CCGCTGATTTGCATAAGGTT-3′) and *Pik3r1* (5′-AGTCGTACAGTGCTCTGTAC-3′) small base-pairing guide RNA. Mice were maintained at the University of Texas Southwestern Medical Center and studies were performed in accordance with institutionally approved protocols. All experiments in this study were approved by the University of Texas Southwestern Medical Center Institutional Animal Care and Use Committee. All mice were fed standard chow (2016 Teklad Global 16% Protein Rodent Diet) except mice with diet-induced obesity, which were fed with control diet (10 kcal% fat; Research Diets) or high-fat diet (60 kcal% fat; Research Diets) from 6 wk of age.

Blood/Serum Chemistries, ELISA, and Insulin Stimulation. Mice were fasted for 6 h (7:00 AM–1:00 PM) for glucose and insulin tests. Blood glucose was tested with the AlphaTRAK glucometer and test strips. ELISA kits were used to measure insulin (Crystal Chem), leptin (Crystal Chem), IGF1 (R&D Systems), and adiponection (B-Bridge) in the serum according to the manufacturer's instructions. AST and ALT in the serum were tested using a Vitros 250 chemistry analyzer (Johnson & Johnson). HbA1c in the whole EDTA blood was measured with a mouse HbA1c assay kit (Crystal Chem). Triglyceride was measured with Infinity Triglycerides Reagent (Thermo Fisher Scientific). The insulin tolerance test was initiated by i.p. injection with human insulin (0.75 U/kg; Sigma-Aldrich) after a 6-h fast. For in vivo insulin stimulation (Fig. S1*J*), insulin or saline was injected i.p. at a dose of 1.5 U/kg body weight after a 6-h fast. Different tissues were collected at 30 min postinjection. For in vivo insulin stimulation (Fig. 6*A*), the mice were fasted for 6 h before surgery. After anesthetization, the skin was opened, and the left iWAT was quickly removed and then snap-frozen in liquid nitrogen. Then 10 U/kg insulin was injected into the portal vein. The iWAT on the right side was taken at 5–6 min after insulin stimulation and frozen in liquid nitrogen. These iWATs were lysed with Nonidet P-40 lysis buffer for IP.

Adipose Transplantation. Transplantation of WT donor fat pads into *Kbtbd2*$^{-/-}$ mice was performed as described previously (38). Details are provided in *SI Materials and Methods*.

Immunohistochemistry and Immunostaining. Samples for routine histology and special stainings were harvested from anesthetized mice and fixed according to standard procedures (39, 40) with modifications for tissue size and stains. Cell immunostaining was performed according to standard protocols. Details are provided in *SI Materials and Methods*.

Cell Culture, Transfection, MEF-Derived Adipocytes, Murine Primary Adipocytes, Human Adipocytes, and shRNA Knockdown. The 293T cells were purchased from American Type Culture Collection (ATCC) and grown at 37 °C in DMEM (Life Technologies)/10% (vol/vol) FBS (Gibco)/antibiotics (Life Technologies) in 5% CO_2. Transfection of plasmids was carried out using Lipofectamine 2000 (Life Technologies) according to the manufacturer's instructions. Cells were harvested between 36 and 48 h posttransfection. MEF cells were isolated using standard protocols by trypsin (Gibco) digestion of minced E13.5 embryos. MEF cells were grown in DMEM/10% (vol/vol) FBS/antibiotics medium. For differentiation, 2-d postconfluent cells (day 0) were treated with grown medium containing 5 μg/mL insulin, 1 μM dexamethasone, 0.5 mM methylisobutylxanthine, and 0.5 μM rosiglitazone (all from Sigma-Aldrich). From day 2, MEF cells were maintained in medium containing 5 μg/mL

insulin (Sigma-Aldrich) and 0.5 μM rosiglitazone (Sigma-Aldrich), which was changed every other day. MEF cells were fully differentiated and harvested at day 10. Isolation and separation of murine primary adipocytes and SVF cells from different adipose tissues (BAT, iWAT) was done as described previously (41). Primary s.c. preadipocytes were purchased from ATCC and grown in complete growth medium (ATCC). Knockdown of *KBTBD2* in human preadipocytes by shRNA was mediated by lentivirus infection following standard protocols. Differentiation was initiated with 2-d postconfluent cells (day 0) with the Adipocyte Differentiation Toolkit for Preadipocytes (ATCC). Fully differentiated adipocytes were harvested at day 15.

Sample Preparation, IP, Ubiquitination, Ub Chain Assay, GST Pull-Down, and Western Blot Analysis. Standard procedures were used for GST pull-down, Western blot analysis, and IP, with modifications for the ubiquitination assay. For two-step IP, anti-FLAG M2 affinity gel (Sigma-Aldrich) was used to purify 3×FLAG-p85α complex in the first-step IP (first IP). Beads from the first IP were eluted with 3×FLAG peptide (Sigma-Aldrich) and then mixed with anti-HA beads (Thermo Fisher Scientific) to purify the HA-Kbtbd2 complex in the second-step IP (second IP). The Ub chain assay was done with the UbiCREST Deubiquitinase Enzyme Kit (Boston Biochem). Further details are provided in *SI Materials and Methods*.

RNA Isolation, Reverse Transcription, and RT-qPCR. Tissue samples were lysed in TRIzol (Invitrogen) for RNA isolation following a standard protocol, and 1 μg of RNA was used for reverse transcription by SuperScript III First-Strand Synthesis SuperMix. RT-qPCR was performed with ABI StepOnePlus with Powerup SYBR Green Master Mix (Life Technologies). The $2^{-\Delta\Delta Ct}$ method was used for relative quantification. The following primer pairs were used: *Kbtbd2*, 5′-ATACCGAATATGCTGTGTCCT-3′ (forward), 5′-AACATGGCCCTGAAATAGGAG-3′ (reverse); *Pik3r1*, 5′-GACATCTCAAGGGAAGAAGTG-3′ (forward), 5′-TTAGTGTAAGAGTGTAATCGCC-3′ (reverse); *Actb*, 5′-CACCACACCTTCTACAATGAG-3′ (forward), 5′-GTCTCAAACATGATCTGGGTC-3′ (reverse).

Mass Spectrometry Analysis of Proteins in Adipose Tissues. Here 100 μg of adipose lysates were loaded onto 12% (wt/vol) SDS/PAGE gel and run ∼1 cm into separation gel. The gel was stained with Coomassie blue, and whole stained lanes were subjected to semiquantitative mass spectrometry analysis (LC/MS/MS), as described in *SI Materials and Methods*.

Statistical Analyses. Data represent mean ± SEM in all graphs depicting error bars. The statistical significance of differences between experimental groups was determined by Student's *t* test using GraphPad Prism 6. $*P \leq 0.05$; $**P \leq 0.01$; $***P \leq 0.001$; $****P \leq 0.0001$; ns, not significant with $P > 0.05$.

ACKNOWLEDGMENTS. We thank Peter Jurek for expert assistance in preparing the figures; Zhe Chen for assistance with MRI; John Shelton, Dr. James A. Richardson, and the staff of the Molecular Pathology Core at the University of Texas Southwestern Medical Center for assistance with histology; and the staff of the Proteomics Core at the University of Texas Southwestern Medical Center for assistance with mass spectrometry. This work was supported by generous donations from the Lyda Hill Foundation and the Kent and JoAnn Foster Family Foundation, and by NIH Grants P01 AI070167 and U19 AI100627.

1. Leney SE, Tavaré JM (2009) The molecular basis of insulin-stimulated glucose uptake: Signalling, trafficking and potential drug targets. *J Endocrinol* 203(1):1–18.
2. Saltiel AR, Kahn CR (2001) Insulin signalling and the regulation of glucose and lipid metabolism. *Nature* 414(6865):799–806.
3. Fritsch R, Downward J (2013) SnapShot: Class I PI3K isoform signaling. *Cell* 154(4): 940–940.e1.
4. Burke JE, et al. (2011) Dynamics of the phosphoinositide 3-kinase p110δ interaction with p85α and membranes reveals aspects of regulation distinct from p110α. *Structure* 19(8):1127–1137.
5. Wu H, et al. (2009) Regulation of class IA PI 3-kinases: C2 domain-iSH2 domain contacts inhibit p85/p110alpha and are disrupted in oncogenic p85 mutants. *Proc Natl Acad Sci USA* 106(48):20258–20263.
6. Yu J, Wjasow C, Backer JM (1998) Regulation of the p85/p110alpha phosphatidylinositol 3′-kinase: Distinct roles for the n-terminal and c-terminal SH2 domains. *J Biol Chem* 273(46):30199–30203.
7. Yu J, et al. (1998) Regulation of the p85/p110 phosphatidylinositol 3′-kinase: Stabilization and inhibition of the p110alpha catalytic subunit by the p85 regulatory subunit. *Mol Cell Biol* 18(3):1379–1387.
8. Zhang X, et al. (2011) Structure of lipid kinase p110β/p85β elucidates an unusual SH2 domain-mediated inhibitory mechanism. *Mol Cell* 41(5):567–578.
9. Carpenter CL, et al. (1993) Phosphoinositide 3-kinase is activated by phosphopeptides that bind to the SH2 domains of the 85-kDa subunit. *J Biol Chem* 268(13):9478–9483.
10. Rordorf-Nikolic T, Van Horn DJ, Chen D, White MF, Backer JM (1995) Regulation of phosphatidylinositol 3′-kinase by tyrosyl phosphoproteins: Full activation requires occupancy of both SH2 domains in the 85-kDa regulatory subunit. *J Biol Chem* 270(8): 3662–3666.
11. Ueki K, et al. (2002) Molecular balance between the regulatory and catalytic subunits of phosphoinositide 3-kinase regulates cell signaling and survival. *Mol Cell Biol* 22(3): 965–977.
12. Ueki K, et al. (2003) Positive and negative roles of p85 alpha and p85 beta regulatory subunits of phosphoinositide 3-kinase in insulin signaling. *J Biol Chem* 278(48): 48453–48466.
13. Luo J, Field SJ, Lee JY, Engelman JA, Cantley LC (2005) The p85 regulatory subunit of phosphoinositide 3-kinase down-regulates IRS-1 signaling via the formation of a sequestration complex. *J Cell Biol* 170(3):455–464.
14. Wang T, et al. (2015) Real-time resolution of point mutations that cause phenovariance in mice. *Proc Natl Acad Sci USA* 112(5):E440–E449.
15. Borén J, Taskinen MR, Olofsson SO, Levin M (2013) Ectopic lipid storage and insulin resistance: A harmful relationship. *J Intern Med* 274(1):25–40.
16. Stogios PJ, Privé GG (2004) The BACK domain in BTB-kelch proteins. *Trends Biochem Sci* 29(12):634–637.
17. Ruan J, et al. (2008) TreeFam: 2008 update. *Nucleic Acids Res* 36(Database issue): D735–D740.
18. NCBI Resource Coordinators (2016) Database resources of the National Center for Biotechnology Information. *Nucleic Acids Res* 44(D1):D7–D19.
19. Furukawa M, He YJ, Borchers C, Xiong Y (2003) Targeting of protein ubiquitination by BTB-Cullin 3-Roc1 ubiquitin ligases. *Nat Cell Biol* 5(11):1001–1007.
20. Cooper MS, Seibel MJ, Zhou H (2016) Glucocorticoids, bone and energy metabolism. *Bone* 82:64–68.
21. Qatanani M, Lazar MA (2007) Mechanisms of obesity-associated insulin resistance: Many choices on the menu. *Genes Dev* 21(12):1443–1455.
22. Kuchay S, et al. (2013) FBXL2- and PTPL1-mediated degradation of p110-free p85β regulatory subunit controls the PI(3)K signalling cascade. *Nat Cell Biol* 15(5):472–480.
23. Bodner M, et al. (1988) The pituitary-specific transcription factor GHF-1 is a homeobox-containing protein. *Cell* 55(3):505–518.
24. Cohen LE, Hashimoto Y, Zanger K, Wondisford F, Radovick S (1999) CREB-independent regulation by CBP is a novel mechanism of human growth hormone gene expression. *J Clin Invest* 104(8):1123–1130.
25. Kishimoto M, et al. (2002) Novel function of the transactivation domain of a pituitary-specific transcription factor, Pit-1. *J Biol Chem* 277(47):45141–45148.
26. Romero CJ, et al. (2012) Insulin-like growth factor 1 mediates negative feedback to somatotroph GH expression via POU1F1/CREB binding protein interactions. *Mol Cell Biol* 32(21):4258–4269.
27. Bondy CA, Cheng CM (2004) Signaling by insulin-like growth factor 1 in brain. *Eur J Pharmacol* 490(1-3):25–31.
28. Thauvin-Robinet C, et al. (2013) PIK3R1 mutations cause syndromic insulin resistance with lipoatrophy. *Am J Hum Genet* 93(1):141–149.
29. Dyment DA, et al.; FORGE Canada Consortium (2013) Mutations in PIK3R1 cause SHORT syndrome. *Am J Hum Genet* 93(1):158–166.
30. Chudasama KK, et al. (2013) SHORT syndrome with partial lipodystrophy due to impaired phosphatidylinositol 3 kinase signaling. *Am J Hum Genet* 93(1):150–157.
31. Chen D, et al. (2004) p50alpha/p55alpha phosphoinositide 3-kinase knockout mice exhibit enhanced insulin sensitivity. *Mol Cell Biol* 24(1):320–329.
32. Fruman DA, et al. (2000) Hypoglycaemia, liver necrosis and perinatal death in mice lacking all isoforms of phosphoinositide 3-kinase p85 alpha. *Nat Genet* 26(3):379–382.
33. Mauvais-Jarvis F, et al. (2002) Reduced expression of the murine p85alpha subunit of phosphoinositide 3-kinase improves insulin signaling and ameliorates diabetes. *J Clin Invest* 109(1):141–149.
34. Terauchi Y, et al. (1999) Increased insulin sensitivity and hypoglycaemia in mice lacking the p85 alpha subunit of phosphoinositide 3-kinase. *Nat Genet* 21(2):230–235.
35. Barbour LA, et al. (2004) Human placental growth hormone increases expression of the p85 regulatory unit of phosphatidylinositol 3-kinase and triggers severe insulin resistance in skeletal muscle. *Endocrinology* 145(3):1144–1150.
36. Ueki K, Algenstaedt P, Mauvais-Jarvis F, Kahn CR (2000) Positive and negative regulation of phosphoinositide 3-kinase–dependent signaling pathways by three different gene products of the p85alpha regulatory subunit. *Mol Cell Biol* 20(21):8035–8046.
37. Ran FA, et al. (2013) Genome engineering using the CRISPR-Cas9 system. *Nat Protoc* 8(11):2281–2308.
38. Klebanov S, Astle CM, DeSimone O, Ablamunits V, Harrison DE (2005) Adipose tissue transplantation protects ob/ob mice from obesity, normalizes insulin sensitivity, and restores fertility. *J Endocrinol* 186(1):203–211.
39. Sheehan DC, Hrapchak BB (1980) *Theory and Practice of Histotechnology* (Battelle Press, Columbus, OH), Ed 2.
40. Woods AE, Ellis RC (1996) *Laboratory Histopathology: A Complete Reference* (Churchill Livingstone, London).
41. Viswanadha S, Londos C (2008) Determination of lipolysis in isolated primary adipocytes. *Methods Mol Biol* 456:299–306.
42. Trudgian DC, Mirzaei H (2012) Cloud CPFP: A shotgun proteomics data analysis pipeline using cloud and high performance computing. *J Proteome Res* 11(12): 6282–6290.
43. Craig R, Beavis RC (2004) TANDEM: Matching proteins with tandem mass spectra. *Bioinformatics* 20(9):1466–1467.
44. Geer LY, et al. (2004) Open mass spectrometry search algorithm. *J Proteome Res* 3(5): 958–964.
45. Elias JE, Gygi SP (2007) Target-decoy search strategy for increased confidence in large-scale protein identifications by mass spectrometry. *Nat Methods* 4(3):207–214.